Compressibility of multicomponent, charged model biomembranes tunes permeation of cationic nanoparticles

Anurag Chaudhury,†,§ Gopal Kishor Varshney,†,§ Koushik Debnath,‡ Gangadhar Das,¶ Nikhil R. Jana,‡ and Jaydeep Kumar Basu∗,†

†Department of Physics, Indian Institute of Science, Bangalore 560012, India

‡School of Materials Science, Indian Association for the Cultivation of Sciences, Kolkata 700032, India

¶KEK-High Energy Accelerator Research Organization, 1-1 Oho, Tsukuba, Ibaraki 305-0801, Japan

§ Contributed equally to this work

E-mail: basu@iisc.ac.in

Phone: +91-80-2293 3281

Fabrication of two-component supported lipid bilayers:

Langmuir-Blodgett/Langmuir-Schaefer (LB/LS) method has been utilized for the deposition of two-component lipid bilayers on silicon substrate. Prior to transfer of bilayer, silicon substrates were made hydrophilic by boiling in a solution of H_2O:NH_4OH:H_2O_2 = 5:1:1 for 10 minutes followed by subsequent rinsing in deionized water several times. A chloroform solution of mixed phospholipids was spread uniformly over the water surface by using a Hamilton syringe. After spreading, the barriers were kept stationary for 15 minutes for complete evaporation of chloroform. The temperature of trough was kept at 20 °C. Surface pressure versus area/molecule isotherms were recorded using the KSV LB rectangular mini Trough (area, 243 cm^2) equipped with a wilhelmy balance. A platinum sensor of accuracy 0.1 mN/m was used to measure the interfacial surface pressure. The barriers were then compressed at a constant rate of 5mm/min to record the isotherms of the monolayers. Fig. 1(a) shows the pressure-area isotherm of these two-component monolayers. Supported lipid bilayers (SLBs) were formed upon controlled transfer of lipid interfacial monolayers onto pretreated silicon substrate. Multiple compression-expansion cycles were carried out during the preparation of bilayers and subsequently they were transferred at a surface pressure of 32 mN/m to the hydrolyzed silicon substrate. The first monolayer was transferred by vertical withdrawal of the substrate at a speed of 5 mm/min. In the monolayer transferred onto the hydrophilic silicon surface, the charged head groups of lipid faced the silicon surface and the hydrophobic hydrocarbon chains were directed towards the air. The second monolayer was transferred at the same surface pressure by a horizontal down stroke on the substrate. After transfer, the SLBs were moved to a container under water and stored at room temperature for further use.

The isothermal compression modulus (β) of the lipid monolayer is calculated by using the equation,

$$\beta = -A\left(\frac{\partial A}{\partial \pi}\right)_T$$

Where, π and A are the measured surface pressure and area per molecule, respectively, at a constant temperature, T= 20 °C. The parameter $\left(\frac{\partial A}{\partial \pi}\right)_T$ is calculated by differentiating the pressure-area isotherm. The isothermal compression modulus used to describe mechanical properties of these monolayers. In addition, higher β value suggests the formation of condensed well-packed monolayer.

Characterization of CQD

We have characterized the size distribution of CQDs using TEM and DLS measurements as shown in Figure S1. Details of the TEM and DLS measurements have been given in the manuscript.

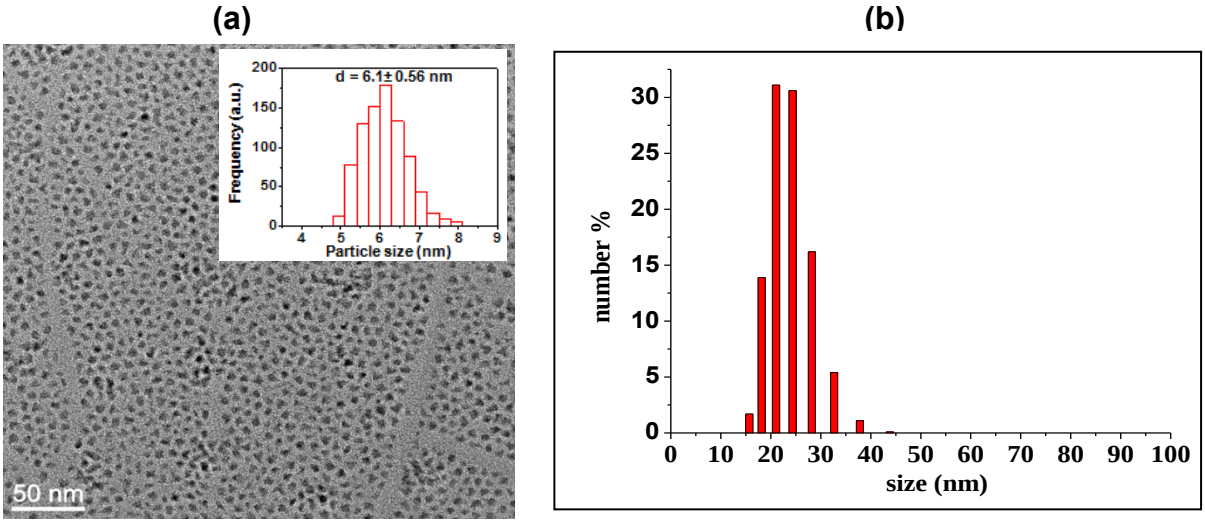

Figure S1: (a) TEM image (along with particle core size (d) distribution at inset) (b) dynamic light based hydrodynamic size distribution of CQDs.

X-ray Reflectivity Measurements:

X-ray reflectivity (XR) measurements were conducted to understand out-of-the-plane structures of these two-component SLBs in detail. These experiments were performed at a synchrotron source. All the XR data from these SLBs were collected at Indian Beamline (BL-18B), Photon Factory, KEK, Japan. The X-ray energy of 16 keV (corresponds to X-ray wavelength = 0.77 Å) was used with a beam of size of 0.15(V) x 1.2(H) mm^2. The scattered beam was collected by a NaI scintillation detector as a function of incident angle. To maintain complete hydration of the SLBs during the measurements, a homemade liquid cell was employed (Figure S2). We utilized the standard reflectivity software (IGOR with motofit package) to analyze the reflectivity curves. The reflectivity curves have been handled as arising from a stack of parallel layers having different thickness and scattering length density depending at the composition.

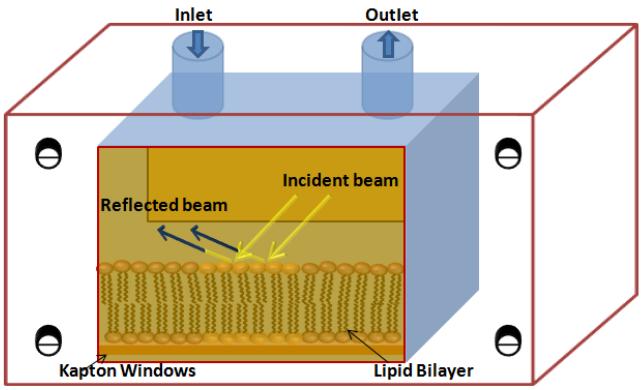

Figure S2: Schematic diagram of supported lipid bilayer deposited on silicon substrate along with the liquid cell used for X-ray reflectivity (XR) measurements.

Different models have been used and compared to fit the experimental XR curves of pure SLBs having different compositions. In presence of CQDs an extra layer consisting of CQD core was taken into consideration. In order to minimize the number of fitting parameters, electron density of water and Si were fixed to 0.334 and 0.713 el/ $Å^3$ respectively. As a metric to quantify the goodness of fit for different models, we have tabulated the Chi squared values in table S1.

For P1G1, XR data were analyzed using Five and six-layered systems (Figure S3). The Five-layered system comprises of (1) outer head groups ($head_2$) in contact with the PBS buffer, (2) outer tails ($tail_2$), (3) inner tails ($tail_1$), (4) inner head groups ($head_1$) and (5) silicon dioxide layer.

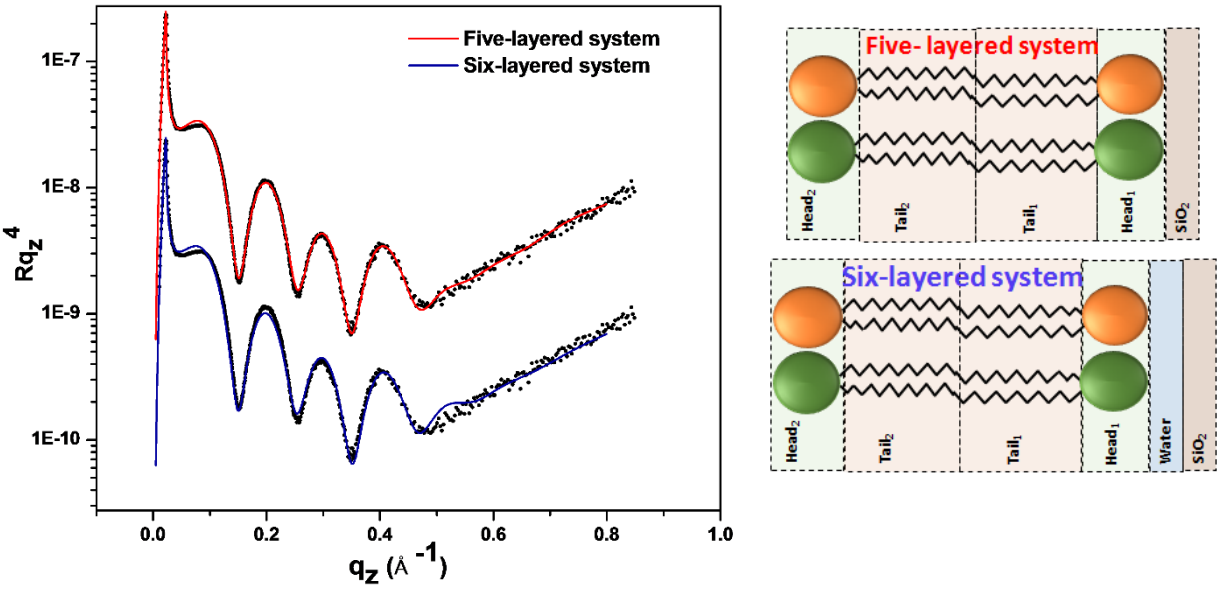

Figure S3: Different XR fitting systems used for the fitting of P1G1 SLBs data. Symbols correspond to the data and solid lines represent the fit. Reflectivity profiles are shifted vertically for clarity.

In case of six-layered model we have added an extra layer of water in between the inner head group and silicon dioxide layer. As shown in Figure S3, a five-layered system could satisfactorily fit the

experimental curves and give physical explanation, therefore it was chosen for further studies related to the interaction of P1G1 with CQDs.

In case of M1G1, Five and two different six-layered systems (designated as 6A and 6B) were used (Figure S4). Five-layered system is same as described above for P1G1. 6A model is analogous in composition as that of Five-layered system, with an extra layer of water between $head_1$ and silicon dioxide. While 6B system contains (1) outer head groups ($head_2$) in contact with the PBS buffer, (2) outer tails ($tail_2$), (3) CH_3 group, (4) inner tails ($tail_1$), (5) inner head groups ($head_1$) and (6) silicon dioxide layer. In our study, the fit of M1G1 is based on a 6B system which is describing the best fit for XR data of M1G1 (Figure S4).

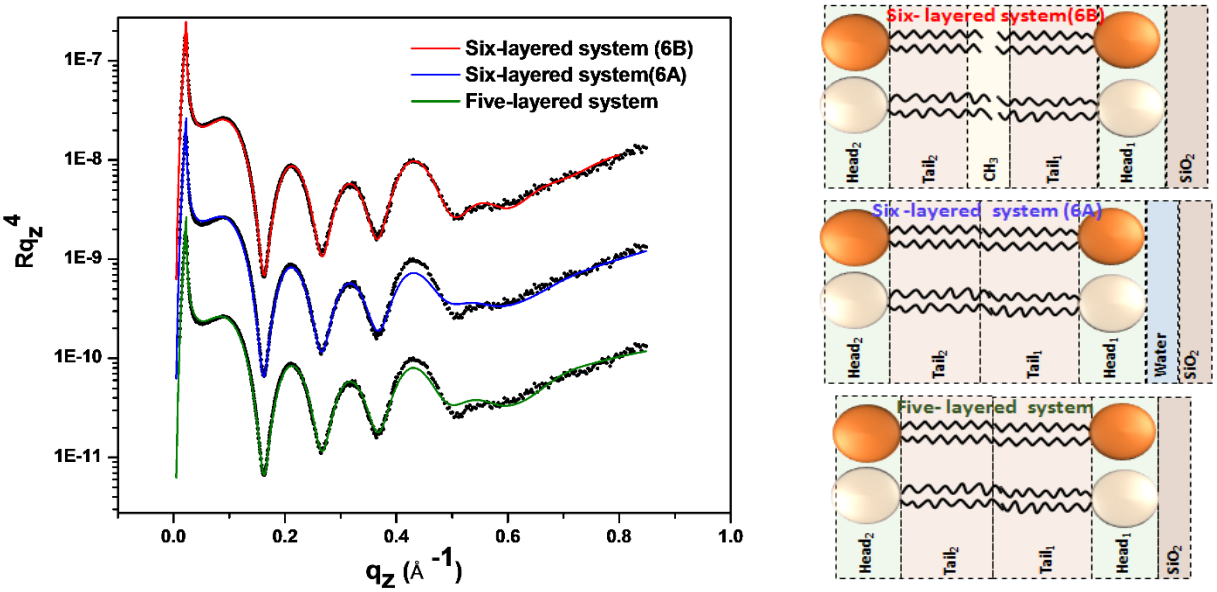

Figure S4: Different XR fitting systems used for the fitting of M1G1 SLBs data. Symbols correspond to the data and solid lines represent the fit. Reflectivity profiles are shifted vertically for clarity.

Five, Six and seven layered systems were used to fit O1G1 SLBs XR data. Five and six layers systems are same as described for P1G1 while in case of seven-layered systems, we split both

upper and lower heads. It is clear from figure S5 that the fits from five and six layered systems were not as good as obtained from the seven-layered system. The latter is having (1) outer head groups of DPPG ($head_{2b}$) in contact with the PBS buffer, (2) outer head groups of DOPC and outer tails ($head_{2a}$ +$tail_2$), (3) outer tails ($tail_2$), (4) inner tails ($tail_1$), (5) inner head groups of DPPG and inner tails ($head_{1b}$+$tail_2$), (6) inner head groups of DOPC ($head_{1a}$) and (7) silicon dioxide, respectively. The best fitting parameters for all these two-component SLBs i.e. thickness and electron density (ED) are summarized in Tables S1-S4.

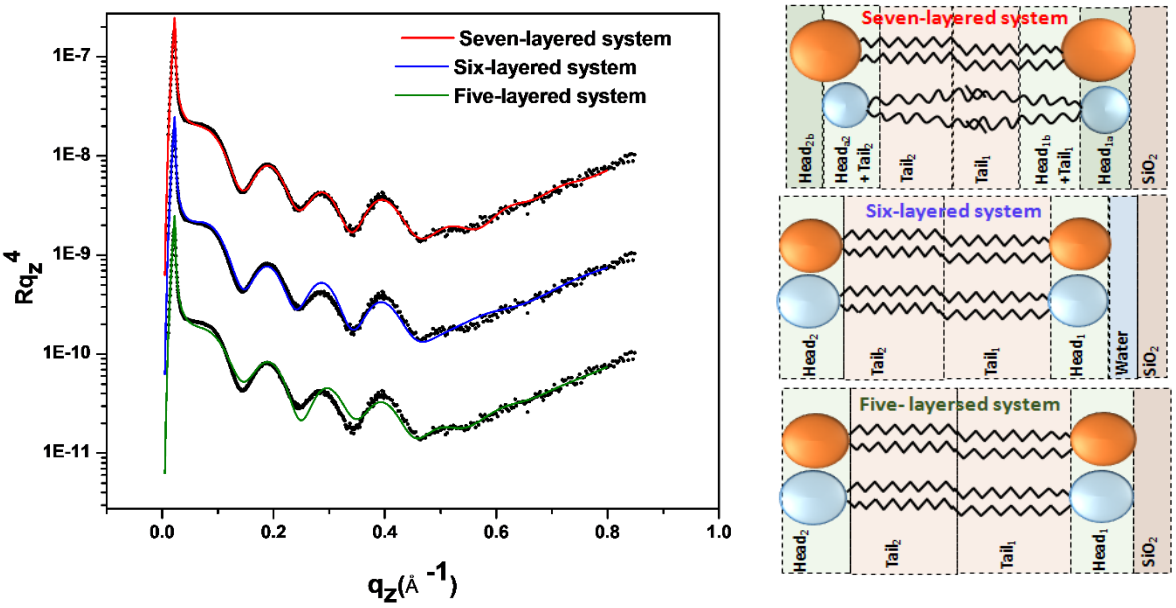

Figure S5: Different XR fitting systems used for the fitting of O1G1 SLBs data. Symbols correspond to the data and solid lines represent the fit. Reflectivity profiles are shifted vertically for clarity.

Atomic force microscopy (AFM) Measurements:

AFM imaging of O1G1 SLBs were performed under water using NT-MDT (Russia) System with a Pyrex-Nitride-Probes-Silicon Nitride (PNP-SiN) cantilever of force constant 0.32 N/m. We used

contact mode imaging with a scan speed of 0.8 Hz for 9 µm X 9 µm. The AFM images were collected from P1G1, M1G1 and O1G1 bilayers transferred on glass substrate at 32 mN/m at 20 $^{\circ}$C. A height difference of ~1 nm between the L_d domain (DOPC in both leaflets) and the ordered DPPG domain (DPPG in both leaflets) could be detected. However, in M1G1 and P1G1, no such height difference between the domains could be detected. The line profiles in (d), (e) show the heights of the P1G1 and M1G1 SLBs measures across a defect, whereas (f) shows the height across the L_o-L_d domains in the O1G1 SLB (c).

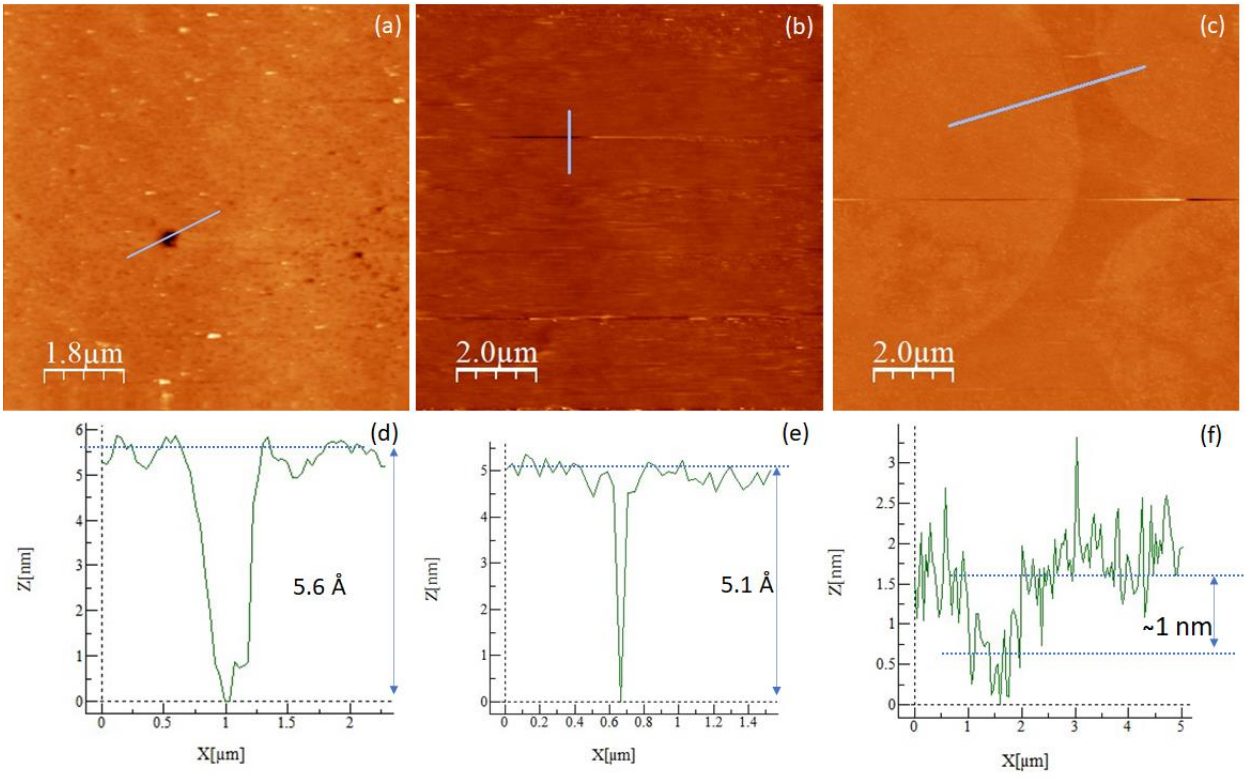

Figure S6: AFM images of (a) P1G1, (b) M1G1 and (c) O1G1 SLBs transferred on glass substrate by LB/LS method. (g)-(i) show the height across the line profile in respective images.

Confocal imaging:

Confocal images were recorded using a commercial Microscopy setup (LEICA TCS SP5 II, GmbH, Mannheim, Germany) with 100X oil objective lens at 640 nM excitation and analyzed by LAS AF microscopy software. To make the bilayer luminescent, dye-tagged lipid (Atto647-DMPE, 0.05 mol %) was added in lipid mixture and mixed thoroughly before spreading at the air-water interface on a Langmuir trough. After transfer of the bilayer onto the glass coverslip using LB/LS technique (described in the Methods section) the bilayers were transferred to a container filled with buffer without exposing to air and stored at 25 °C and used as such. For imaging, 512 × 512 pixels at a 600 Hz frame rate was used for image acquisition. The images reveal phase separation between the domains in the bilayers. The nature of the domains could be readily identified from the O1G1 and M1G1 images. Although the confocal image of P1G1 undoubtedly pertains to phase separation, yet the uneven dye-partitioning, owing to very high isothermal compression modulus/rigidity of the membrane, do not clearly tell about the true nature of the domains.

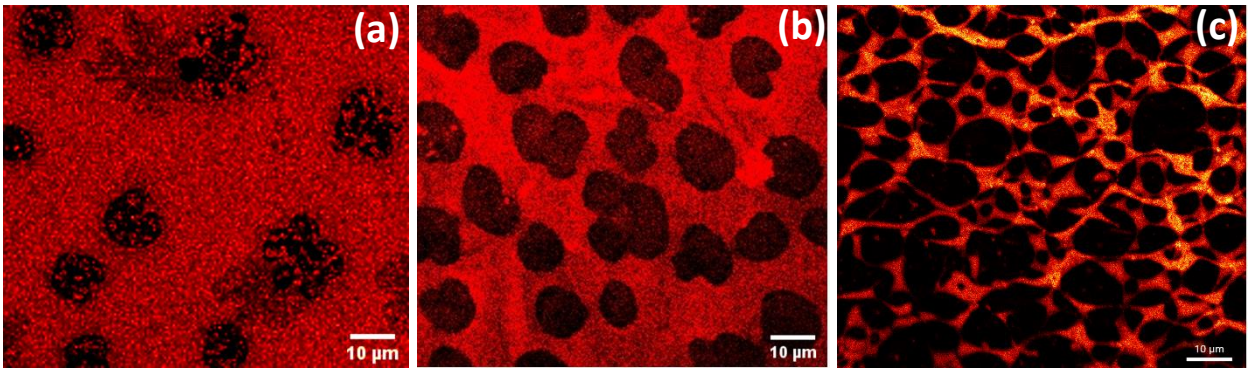

Figure S7: The confocal microscopy images of P1G1, M1G1 and O1G1 SLBs respectively (a-c). The lighter regions are dye rich and the darker region are dye poor region. All the bilayers are stained with Atto647N DMPE (0.05mol %).

Table S1: Chi squared values for different models.

	χ^2
P1G1 5-layered system	47.89
P1G1 6-layered system	157.04
P1G1+ 5nM CQD	35.49
P1G1+ 5nM CQD_NO CQD layer	48.62
P1G1+ 10nM CQD	22
P1G1+ 10nM CQD_NO CQD layer	217.75
M1G1 5-layered system	41.56
M1G1 6-layered system	23.22
M1G1+ 5nM CQD	23.46
M1G1+ 5nM CQD_NO CQD layer	140.15
M1G1+ 10nM CQD	17.08
M1G1+10nM CQD_NO CQD layer	35.07
O1G1 5-layered system	71
O1G1 6-layered system	62
O1G1 7-layered system	32
O1G1+ 5nM CQD	31
O1G1+ 5nM CQD_NO CQD layer	35.24
O1G1+ 10nM CQD	43.98
O1G1+10nM CQD_NO CQD layer	99.98
O1G1+ 5nM CQD_pH5.9	20.46
O1G1+ 5nM CQD_NO CQD layer_pH5.9	90.72

Table S2: Parameters obtained from the fits of X-ray reflectivity data for P1G1 at pH 7. t_n, ρ_n denote the thickness and electron density of the different layers.

layer	Only P1G1		P1G1+5nM CQD		P1G1+10nM CQD	
	t_n (Å)	ρ_n (el/Å ^{3})	t_n (Å)	ρ_n (el/Å ^{3})	t_n (Å)	ρ_n (el/Å ^{3})
Water	INF	0.334	INF	0.334	INF	0.334
CQD	----	----	14.87	0.344	13.29	0.363
head$_2$	9.77	0.439	9.55	0.436	9.19	0.327
tail$_2$	18.94	0.283	17.42	0.301	14.09	0.284
tail$_1$	20.84	0.266	20.77	0.292	15.81	0.297
head$_1$	9.95	0.448	9.89	0.447	9.55	0.411
SiO_2	5.98	0.656	5.98	0.656	5.98	0.656
Si	INF	0.713	INF	0.713	INF	0.713

Table S3: Parameters obtained from the fits of X-ray reflectivity data for M1G1at pH 7. t_n, ρ_n denote the thickness and electron density of the different layers.

layer	Only M1G1		M1G1+ 5nM CQD		M1G1+10nM CQD	
	t_n (Å)	ρ_n (el/Å ^{3})	t_n (Å)	ρ_n (el/Å ^{3})	t_n (Å)	ρ_n (el/Å ^{3})
Water	INF	0.334	INF	0.334	INF	0.334
CQD	-----	----	9.63	0.339	13.04	0.343
head$_2$	9.77	0.431	9.44	0.402	8.79	0.328
tail$_2$	17.19	0.318	15.17	0.314	10.01	0.321
CH_3	1.34	0.207	5.56	0.199	5.54	0.330
tail$_1$	17.99	0.312	15.78	0.316	11.16	0.335
head$_1$	10.55	0.453	10.06	0.420	10.09	0.429
SiO_2	5.69	0.656	5.69	0.656	5.69	0.656
Si	INF	0.713	INF	0.713	INF	0.713

Table S4: Parameters obtained from the fits of X-ray reflectivity data for O1G1 pH7. t_n, ρ_n denote the thickness and electron density of the different layers.

layer	Only O1G1		O1G1+5nM CQD		O1G1+10nM CQD	
	t_n (Å)	ρ_n (el/Å ^{3})	t_n (Å)	ρ_n (el/Å ^{3})	t_n (Å)	ρ_n (el/Å ^{3})
Water	INF	0.334	INF	0.334	INF	0.334
lipidcomplex	----	----	----	----	17.68	0.314
CQD	----	----	10.68	0.33605	----	----
$head_{2b}$	5.89	0.394	6.34	0.371	4.49	0.325
$head_{2a}$ +$tail_2$	7.86	0.426	8.58	0.379	4.11	0.328
$tail_2$	12.70	0.216	12.88	0.176	7.12	0.298
$tail_1$	13.50	0.311	12.81	0.316	7.92	0.270
$head_{1b}$+$tail_1$	5.22	0.462	5.54	0.454	3.52	0.296
$head_{1a}$	8.35	0.440	8.51	0.455	5.10	0.410
SiO_2	14	0.649	14	0.649	14	0.649
Si	INF	0.713	INF	0.713	INF	0.713

Table S5: Parameters obtained from the fits of X-ray reflectivity data for O1G1at pH 5.9. t_n, ρ_n denote the thickness and electron density of the different layers.

layer	Only O1G1		O1G1+5nM CQD	
	t_n (Å)	ρ_n (el/Å ^{3})	t_n (Å)	ρ_n (el/Å ^{3})
Water	INF	0.334	INF	0.334
CQD	----	----	16.83	0.350
$head_{2b}$	5.31	0.412	4.77	0.328
$head_{2a}$ +$tail_2$	7.48	0.450	6.29	0.326
$tail_2$	11.03	0.167	10.45	0.303
$tail_1$	11.72	0.245	10.91	0.277
$head_{1b}$+$tail_1$	5.46	0.417	4.93	0.258
$head_{1a}$	7.56	0.438	5.51	0.408
SiO_2	10.81	0.639	10.81	0.639
Si	INF	0.713	INF	0.713